Space Weather
Lecture 5: Bow Shock

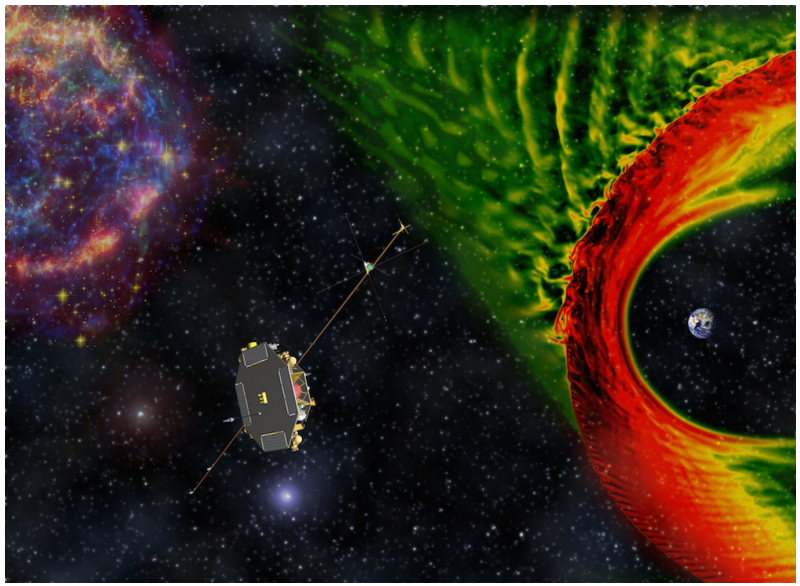

Elena Kronberg (room 442)
elena.kronberg@lmu.de

Introduction: Shock wave

A disturbance that travels faster than the local sound speed (or, in general, a characteristic wave speed) is a *shock wave*.

Sn 1006 brightest supernovae ever

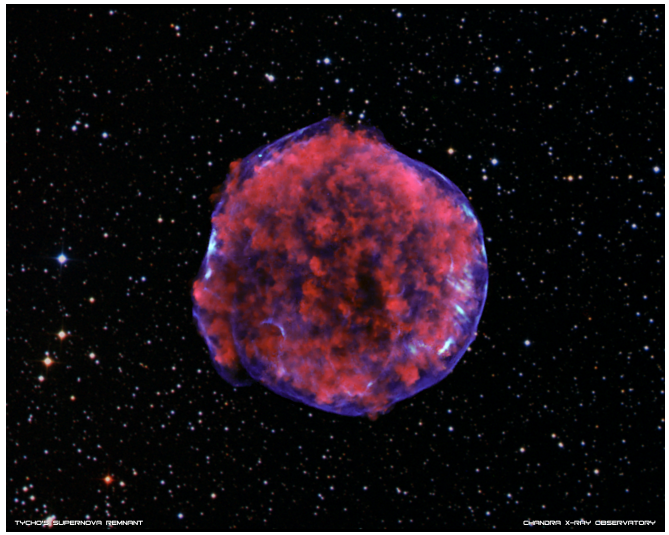

X-43 fastest aircraft

Tail of diplodocus exceeded speed of sound, ~1200 km/h

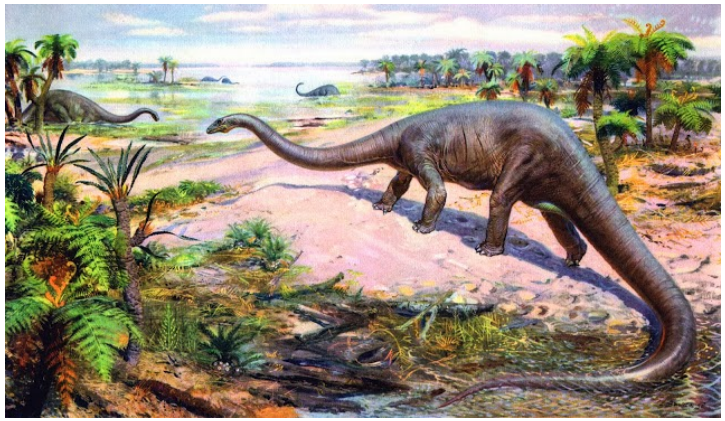

Pistol shrimp, kills enemies at distance by releasing a sound reaching 218 decibels

Introduction: Sound and Alfvén speeds

- The *sound speed* is

$$c_s = (\gamma p/\rho)^{1/2},$$

where γ is the ratio of specific heat, p is the gas pressure and ρ is the mass density. This is the characteristic speed at which information is transmitted through non-ionized, non-magnetic gases.

- The *Alfvén speed* is

$$V_A = \frac{B}{\sqrt{\mu_0 \rho}}.$$

This is the characteristic speed at which information is transmitted along a magnetic field in a plasma.

Introduction: Slow and fast magnetosonic speed (ms)

The MHD equations yield several types of waves:

$$c^2_{\mathrm{ms\,slow}} = \frac{1}{2}\left[\left(c_s^2 + V_A^2\right) - \sqrt{\left(c_s^2 + V_A^2\right)^2 - 4c_s^2 V_A^2 \cos^2\theta_{Bn}}\right],$$

$$c^2_{\mathrm{ms\,fast}} = \frac{1}{2}\left[\left(c_s^2 + V_A^2\right) + \sqrt{\left(c_s^2 + V_A^2\right)^2 - 4c_s^2 V_A^2 \cos^2\theta_{Bn}}\right],$$

where θ_{Bn} is the angle between the incoming magnetic field and the shock normal vector.

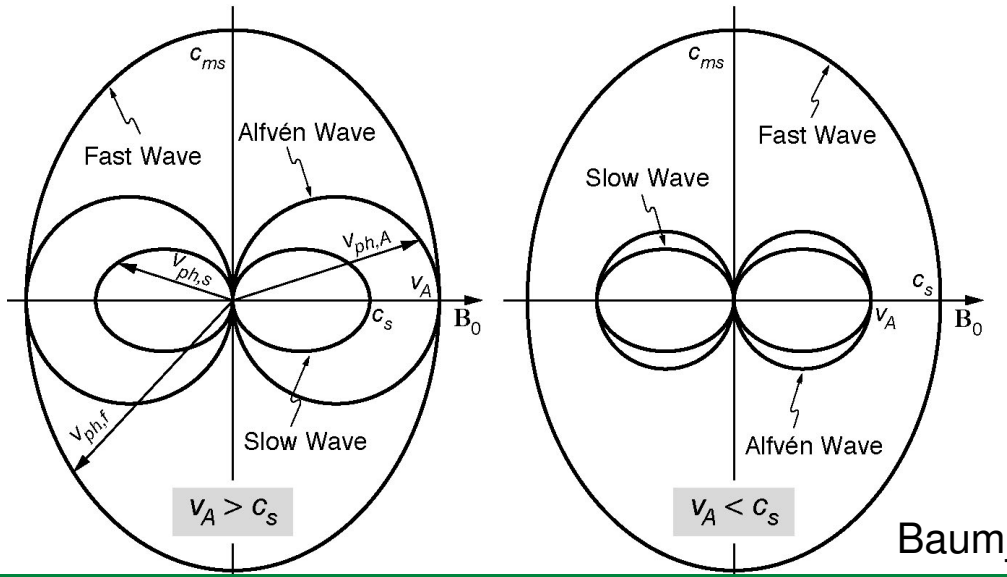

Baumjohann&Treumann 1996

Introduction: Mach numbers

- Sonic Mach number is

$$M_{\mathrm{s}} = \frac{v}{c_{\mathrm{s}}},$$

  where v is fluid velocity.
- Slow Magnetosonic Mach number is

$$M_{\mathrm{ms\,slow}} = \frac{v}{c_{\mathrm{ms\,slow}}}$$

- Alfvén Mach number is

$$M_{\mathrm{A}} = \frac{v}{V_{\mathrm{A}}}$$

- Fast Magnetosonic Mach number is

$$M_{\mathrm{ms\,fast}} = \frac{v}{c_{\mathrm{ms\,fast}}}$$

Introduction: Shock

Shocks are transition layers where the plasma properties change from one equilibrium state to another.
The relation between the plasma properties on both sides of a shock can be obtained from the conservative form of the MHD equations, assuming conservation of mass, momentum, energy, $\partial B/\partial t = \nabla \times (v \times B)$ and of $\nabla \cdot \mathbf{B} = 0$.

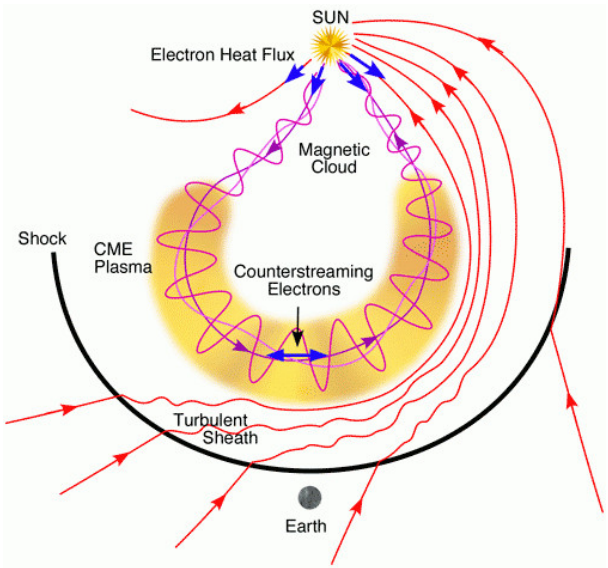

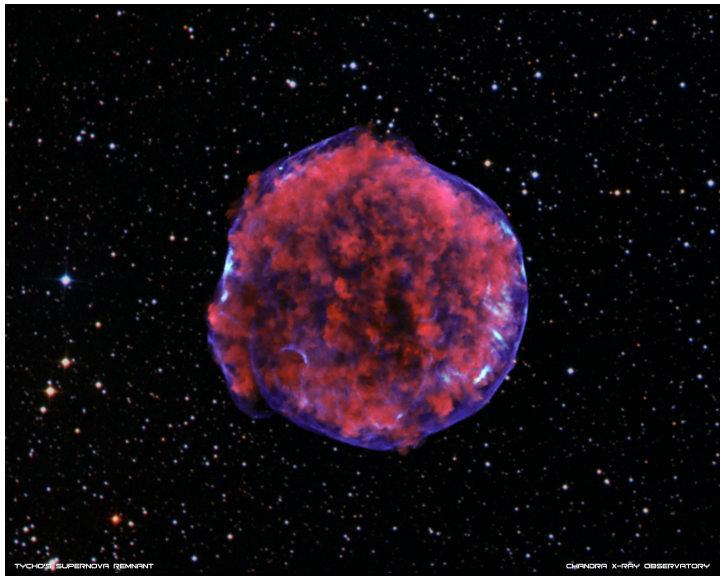

Shock-Conservation Relations

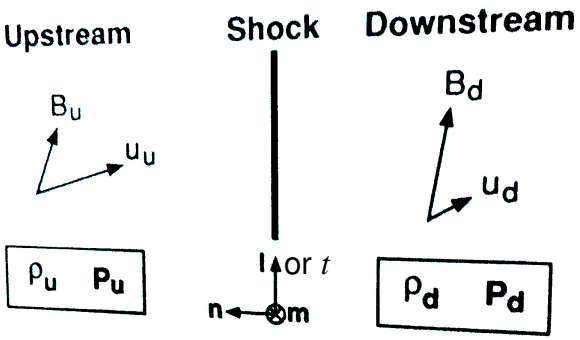

- The jump across the shock in any quantity X:

$$[X] = X_u - X_d$$

- For any quantity, a conservation equation is

$$\frac{\partial Q}{\partial t} + \nabla \cdot F = 0,$$

where Q and F are the density and flux of any conserved quantity. If shock is steady and one-dimensional (variations only along n-axis), then

$$\frac{\partial F_n}{\partial n} = 0.$$

The component of the conserved flux normal to the shock is constant

$$[F_n] = 0.$$

For MHD, the conservation of mass in one dimesion is $\frac{\partial \rho v_n}{\partial n} = 0$ which leads to the jump condition for the shock: $[\rho v_n] = 0$.

Rankine-Hugoniot jump conditions for ideal MHD

$$[B_n]_u^d = 0 \tag{1}$$

$$[v_n B_t - v_t B_n]_u^d = 0 \tag{2}$$

$$[\rho v_n]_u^d = 0 \tag{3}$$

$$[\rho v_n^2 + p + B_t^2/2\mu_0]_u^d = 0 \tag{4}$$

$$[\rho v_n v_t - B_n B_t/\mu_0]_u^d = 0 \tag{5}$$

$$\Big[\frac{1}{2}\rho v^2 v_n + \frac{\gamma}{\gamma-1}\rho v_n + \frac{B_t(v_n B_t - v_t B_n)}{\mu_0}\Big]_u^d = 0 \tag{6}$$

Fast Shocks: $M_{\mathrm{ms\,fast}} > 1$

- Plasma pressure and field strength (Alfvén speed) increase downstream of shock; magnetic field bends away from normal
- Fast shocks are by far the most frequent types of shocks observed in solar-system plasmas (Earth's bow shock. . .)

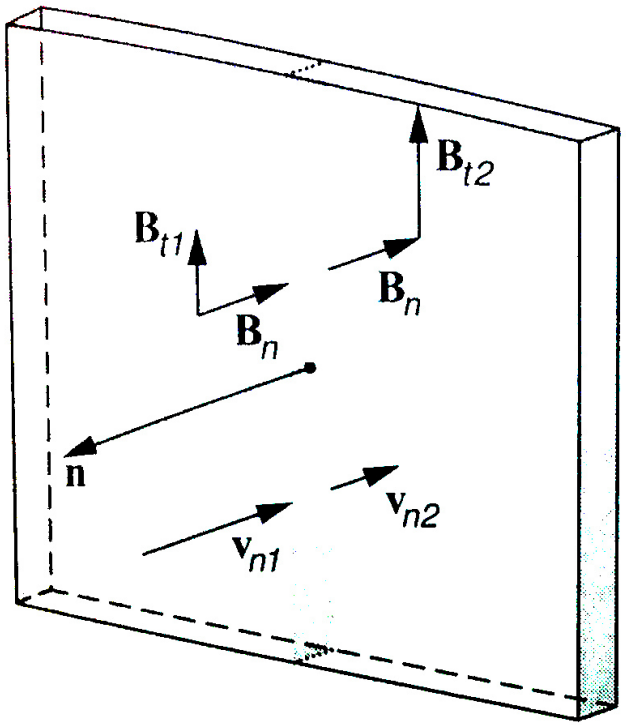

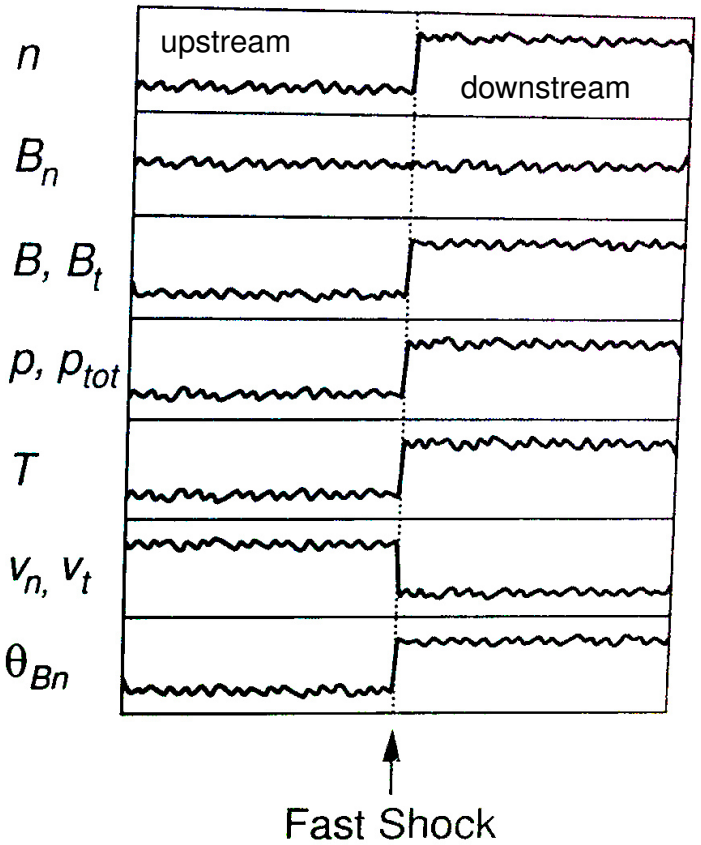

Bow Shock: definition

- The most famous example of a plasma shock is the Earth's bow shock.
- It develops as a result of the interaction of the Earth's magnetosphere with the supersonic solar wind.
- When $M_{ms} > 1$ and the plasma flow is distorted due to the presence of a non-moving object, a shock front will develop across which the fluid quantities will jump discontinuously.
- The super-magnetosonic flow will become sub-magnetosonic.

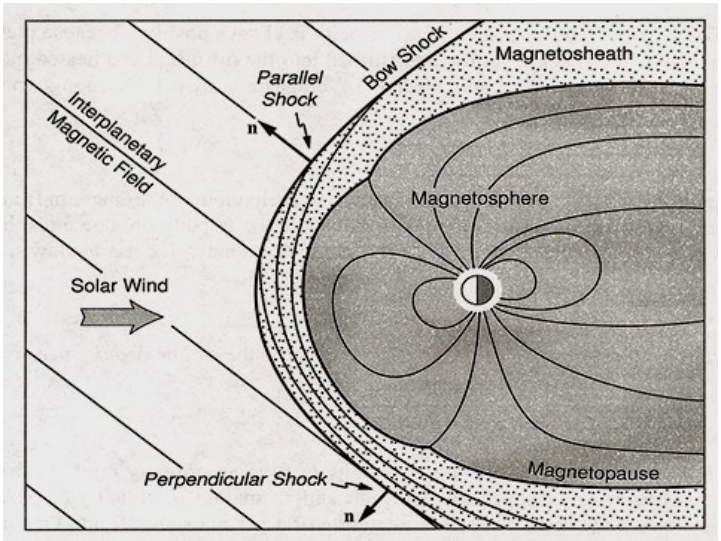

Bow Shock: characteristics

- The surface of the bow shock is parabolically shaped, $M_{ms} \simeq 8$.
- Mach number is defined by the solar wind velocity component normal to the shock, $v_n = v_{sw} \cos\theta$. The condition $M_{ms} > 1$ is satisfied when $\theta < \arccos M_{ms}^{-1}$. Therefore, bow shock forms at $\theta_{max} \simeq 80°$.
- Bow shock divides the solar wind flow into two regions: the undisturbed region upstream of the bow shock and the disturbed magnetosheath flow on the downstream side.

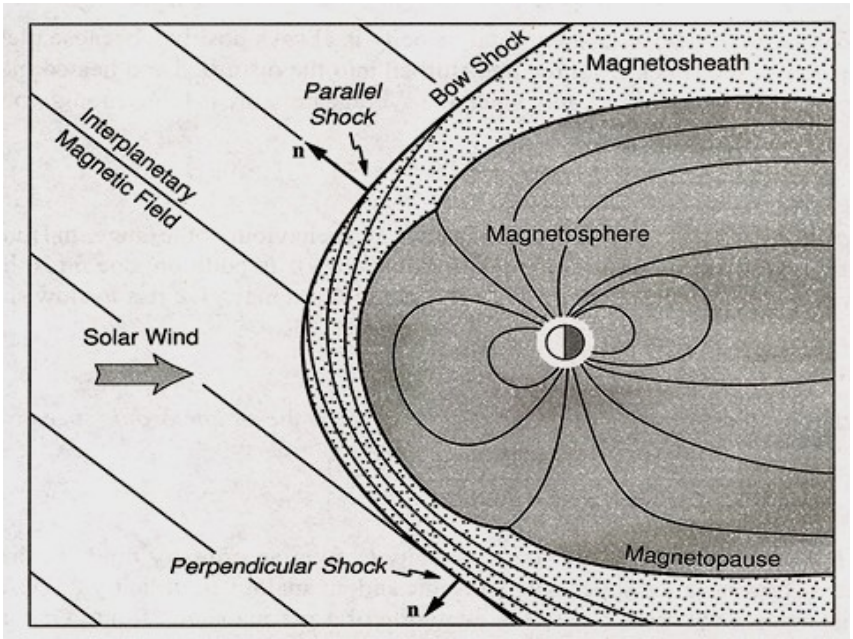

Shape of the bow shock: Mach cone

- In case $V_A \gg c_s$, the Alfvén Mach cone angle defines the shape

$$\theta_A = \arcsin\left(\frac{V_A}{v_{sw}}\right) = \arcsin M_A^{-1}$$

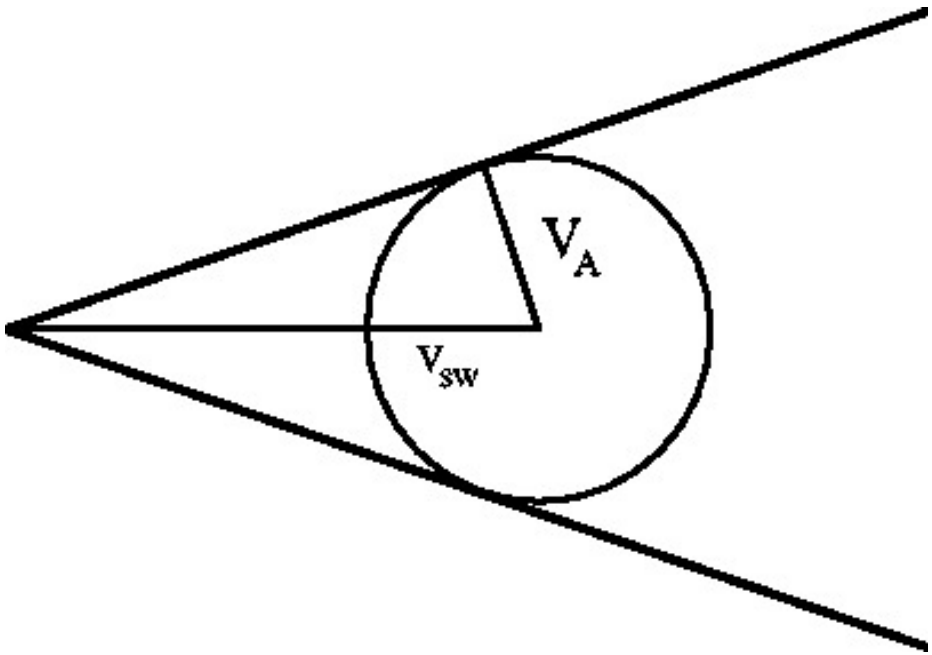

M_A =9.7 (solid), 4.9 (dashed), 1.9 (dotted),1.4 (fancy)

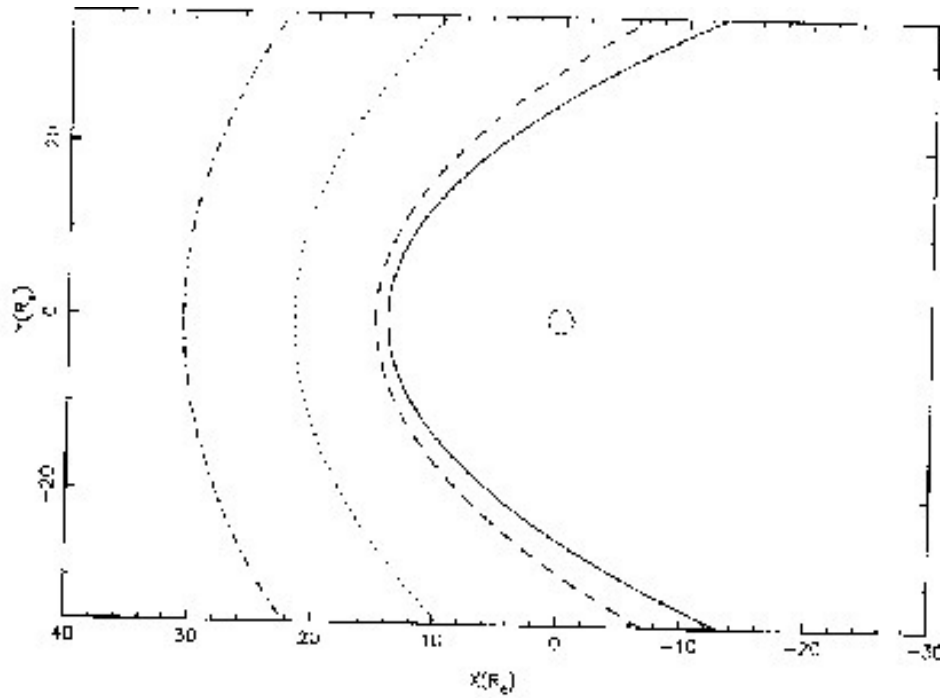

Cairns and Lyon, 1996

Position of the bow shock and magnetosheath

- The position of the bow shock highly varies depending on solar wind dynamic pressure, IMF and M_A (e.g. model by Peredo+95).

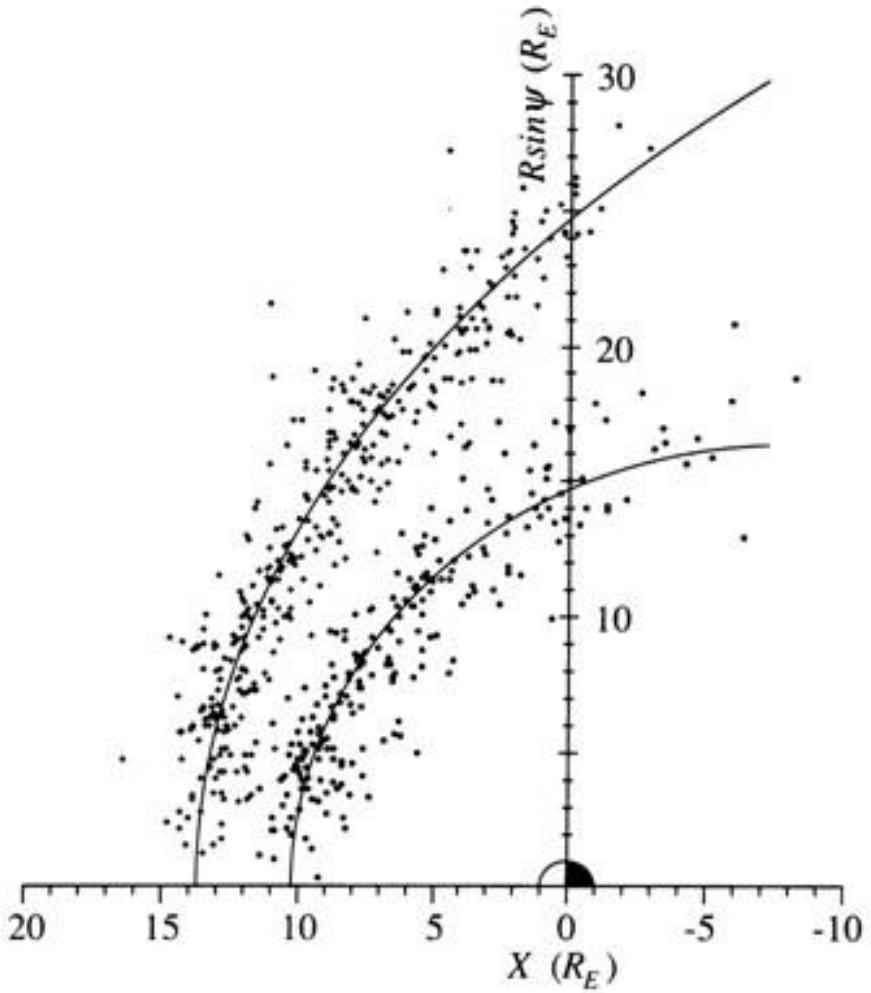

Formation of the bow shock

Vlasiator simulations: Plasma density, IMF at 30°

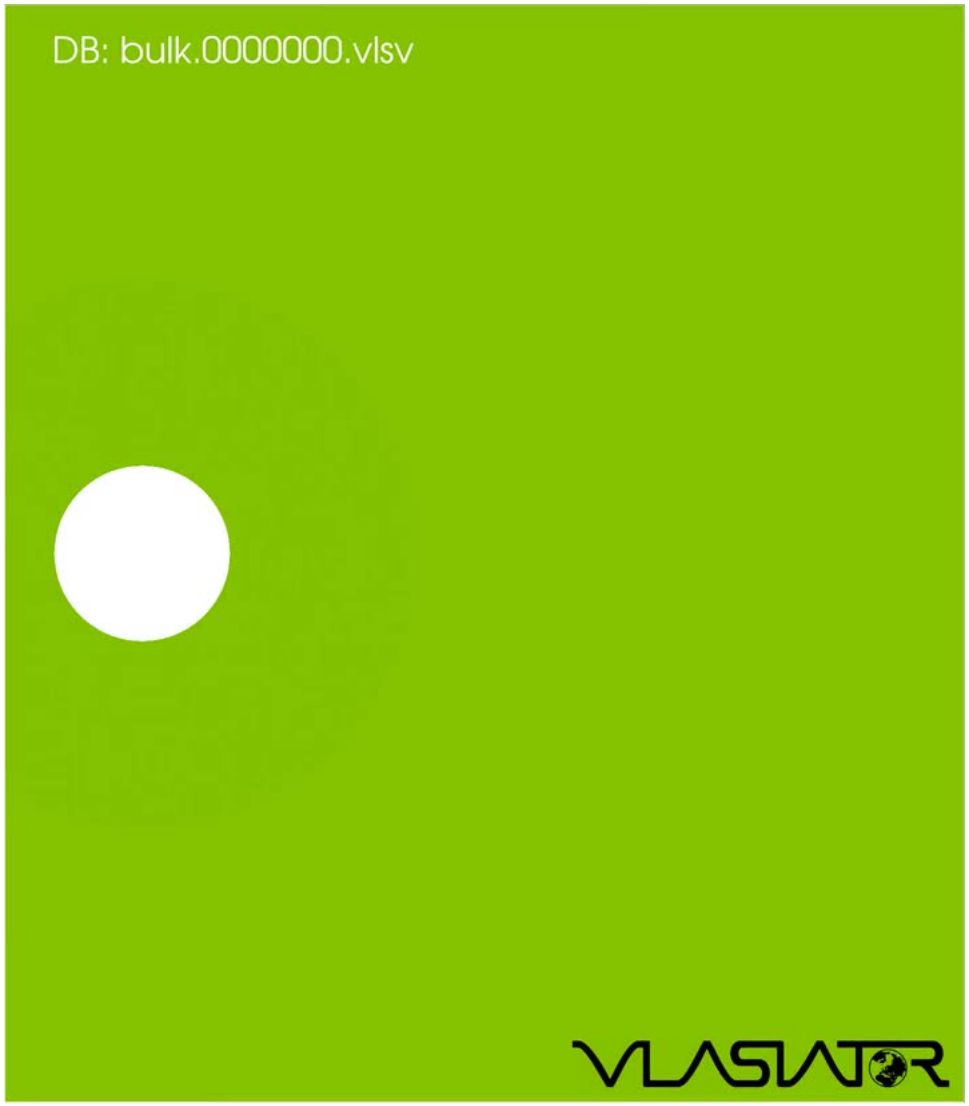

Formation of the bow shock

Vlasiator simulations: Magnetic field magnitude, IMF at 5°

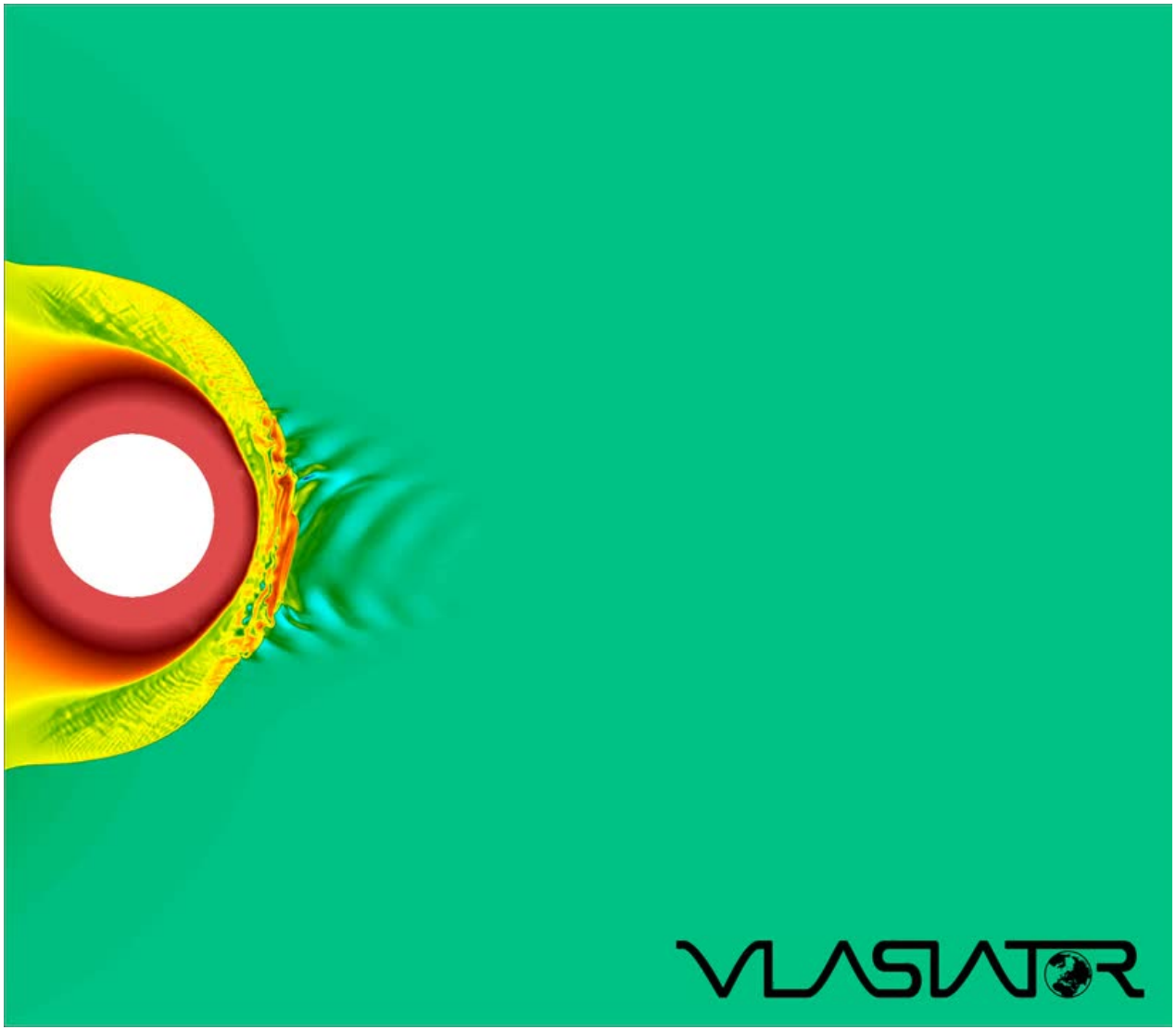

Slow shocks: $M_{\mathrm{ms\,slow}} > 1$

- Plasma pressure increases; magnetic field strength (Alfvén speed) decreases; magnetic field bends toward normal

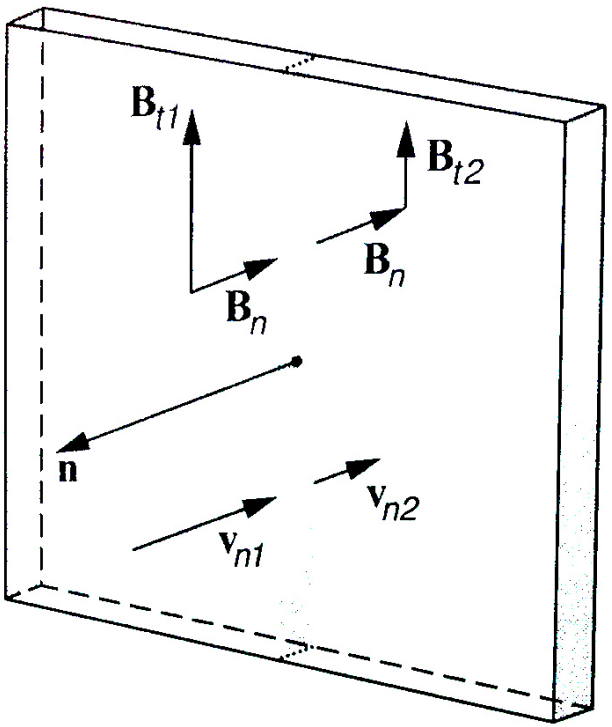

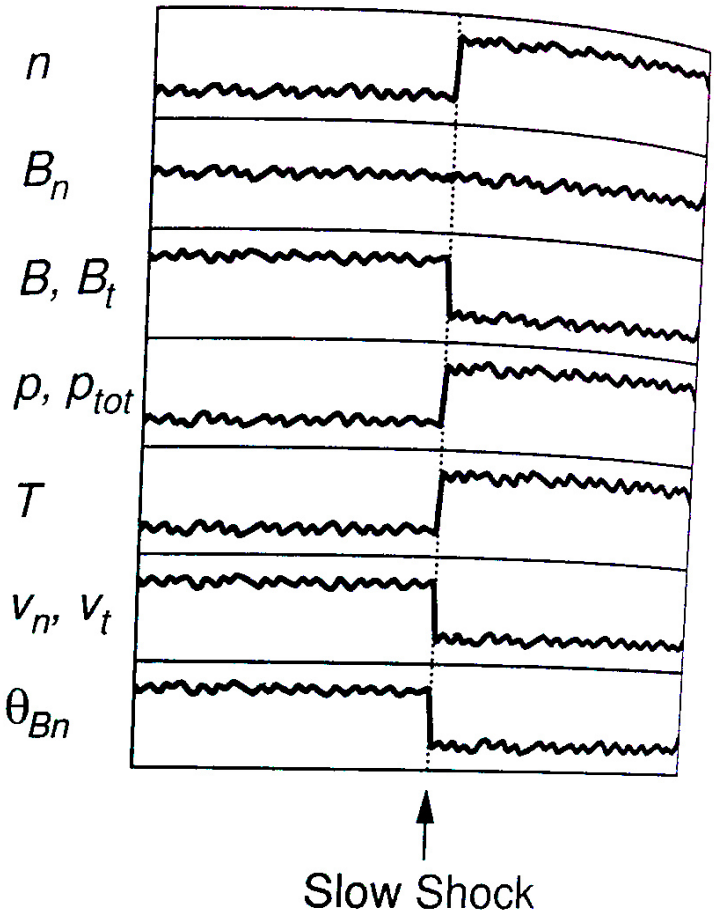

Slow shocks

Petscheck magnetic reconnection is associated with a slow-mode shock; can be related to magnetic reconnection in the solar corona.

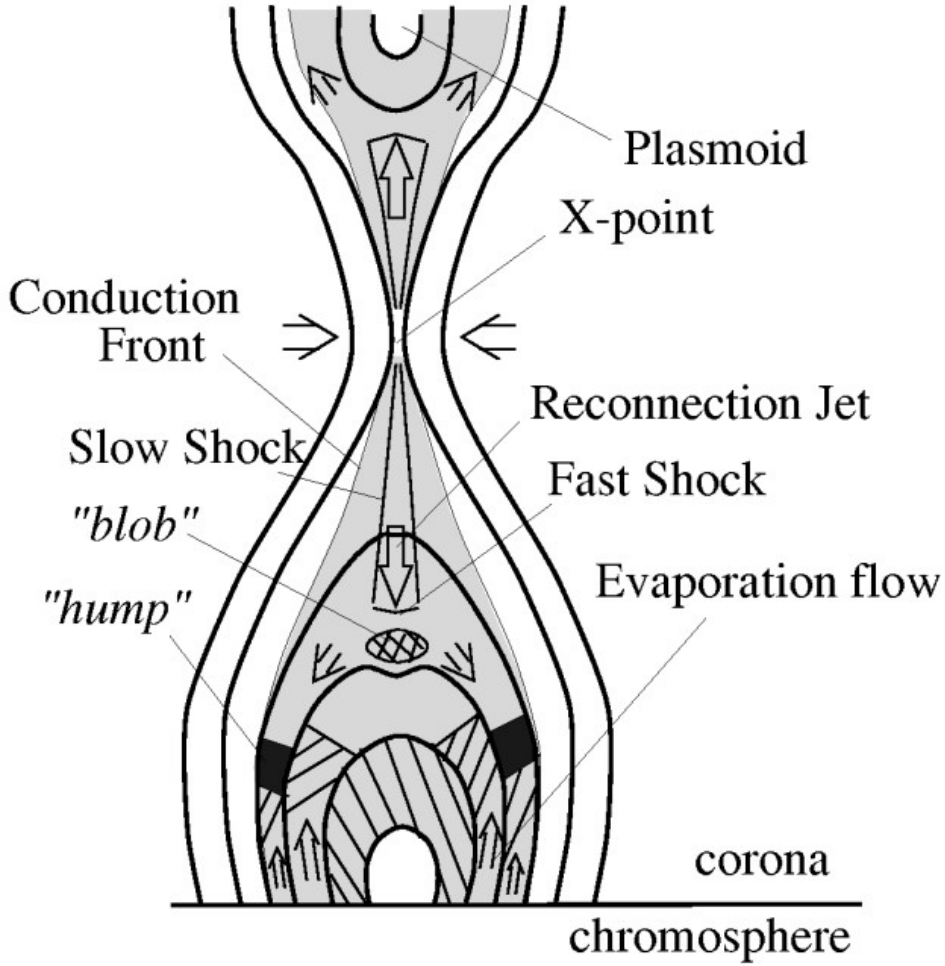

Parallel and perpendicular shocks

- Strictly in parallel shocks the magnetic field is not affected by the shock.
- Realistic parallel shocks are always quasi-parallel and therefore affect the magnetic field amplitude.
- The shock becomes turbulent.

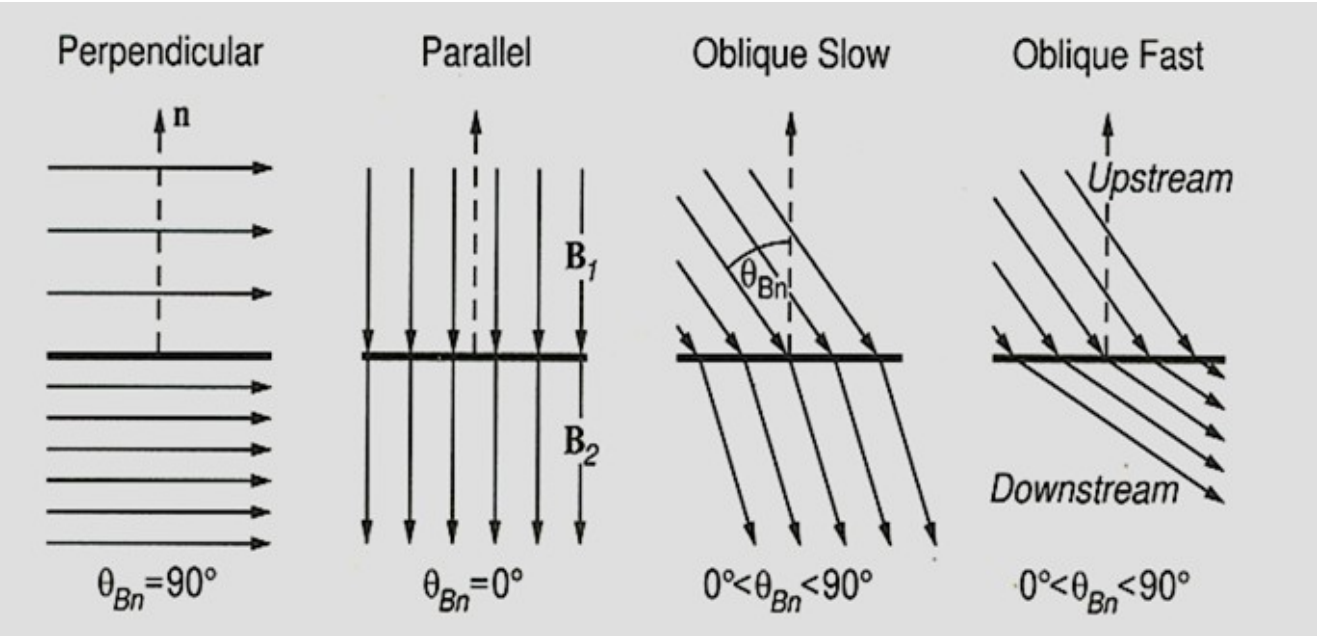

Parallel and perpendicular shocks

- Typical magnetic shock profiles

The field has a sharp jump called the ramp preceded by a gradual rise called the foot. The field right behind the shock is higher than its eventual downstream value. This is called the overshoot.

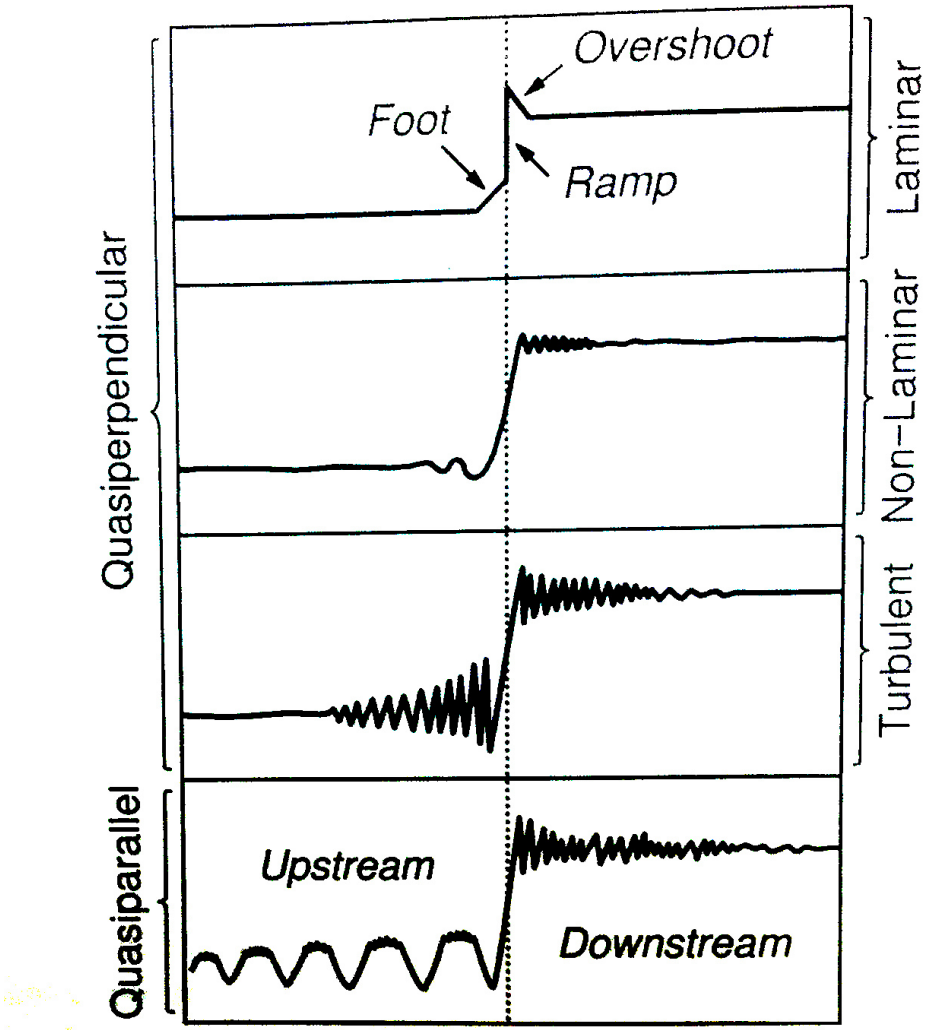

A laminar fluid flows in parallel layers, with no disruption between the layers

Parallel and perpendicular shocks

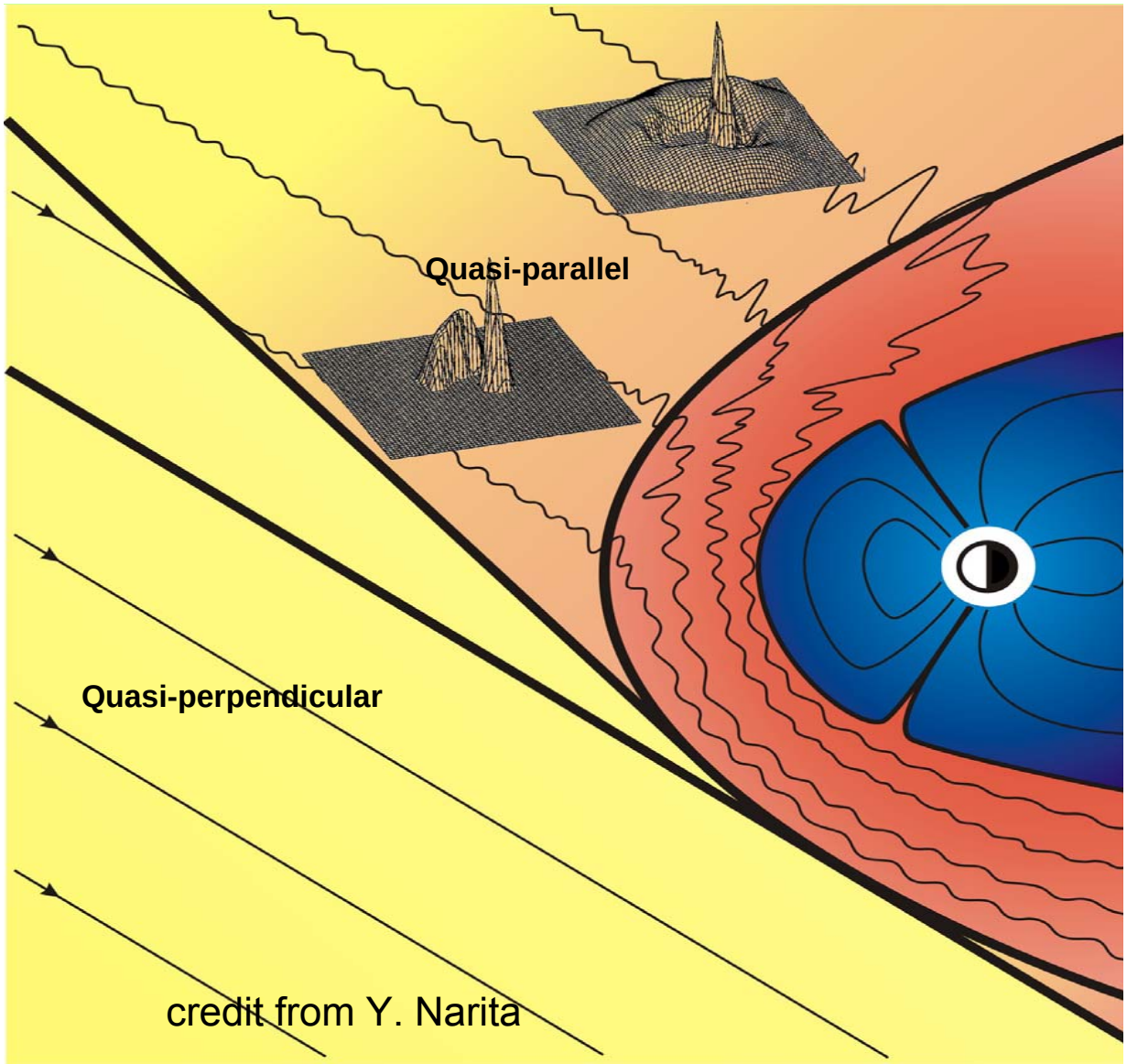

Parallel and perpendicular shocks: magnetic field

The positions of the quasi-parallel and quasi-perpendicular shock regions move due to the change in the IMF direction.

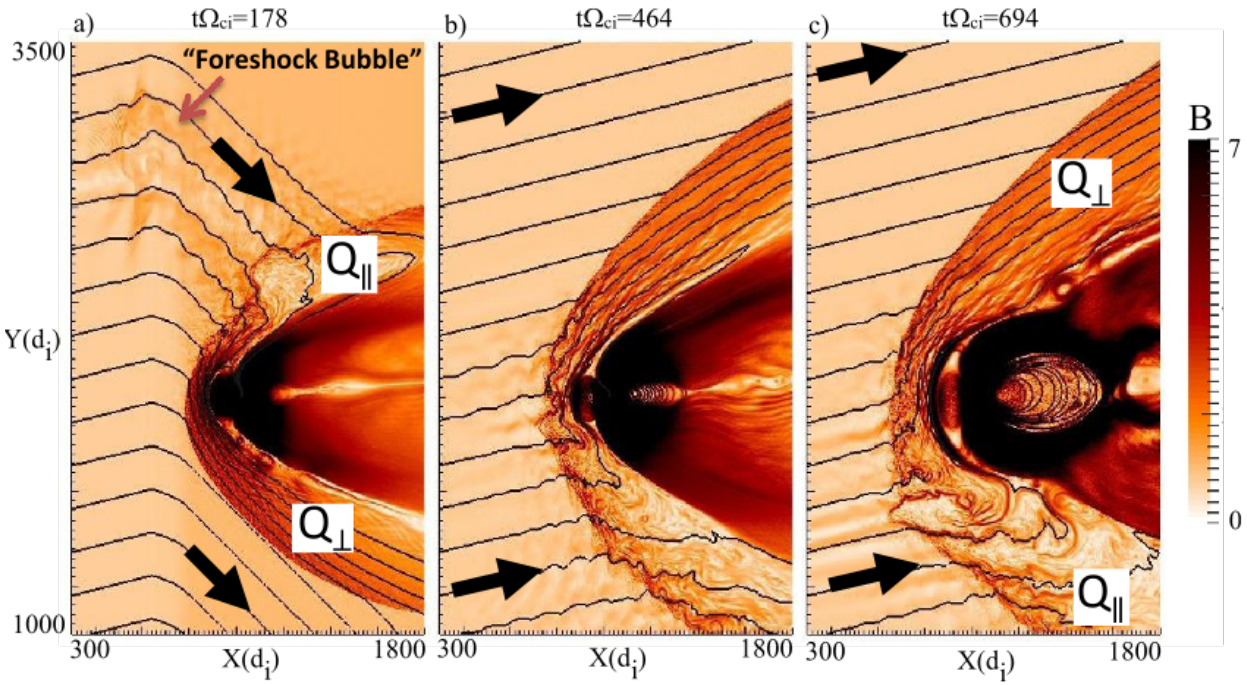

Karimabadi+14

Quasi-parallel and quasi-perpendicular shocks: temperature

The enhanced heating in the quasi-parallel as compared to quasi-perpendicular magnetosheath is clearly evident.

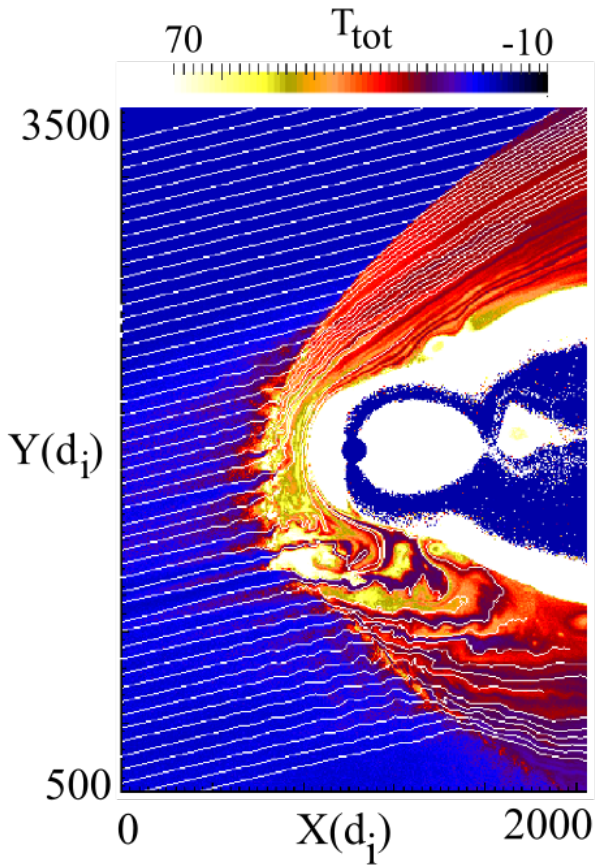

Karimabadi+14

Tools to study bow shock

To study the solar wind-Earth interaction we have an excellent tool: mission CLUSTER

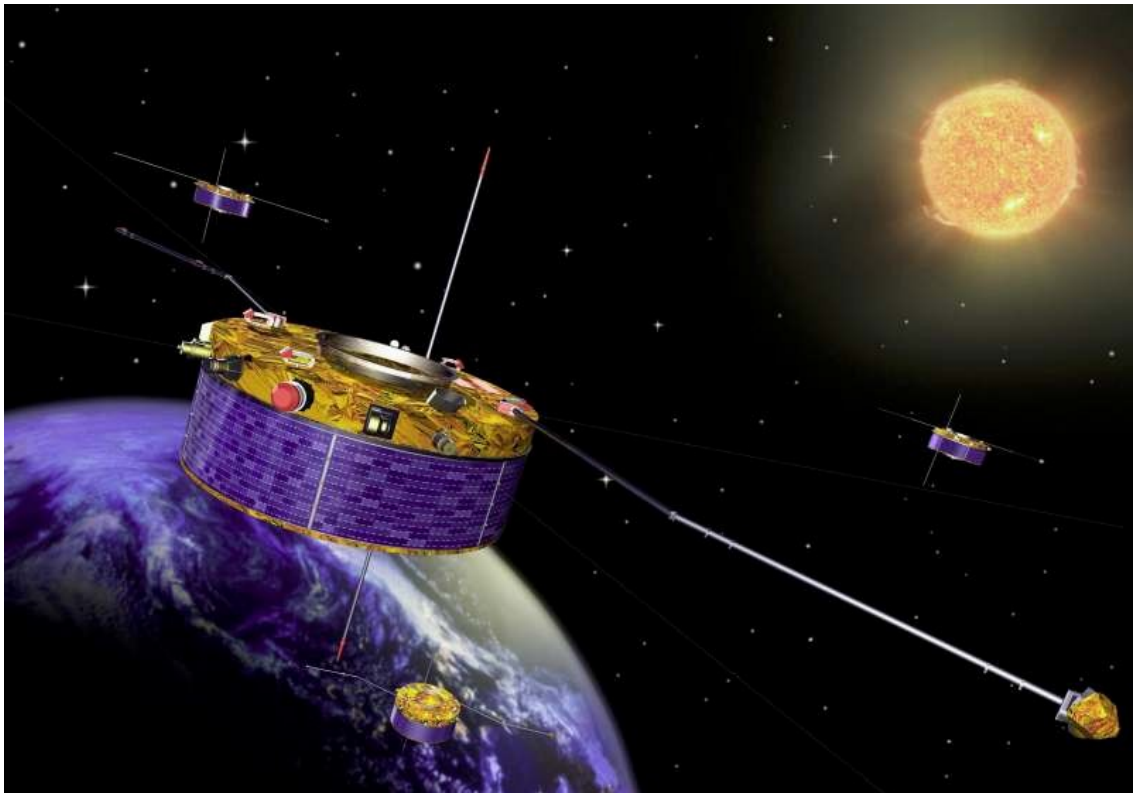

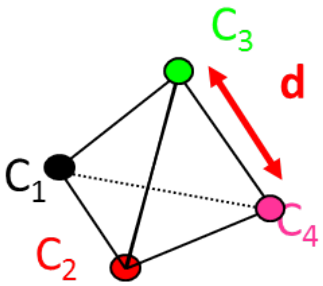

Cluster orbits 2001–2012

"Orbits are traversing the regions of prime interest in the magnetosphere, both at high and low latitudes."

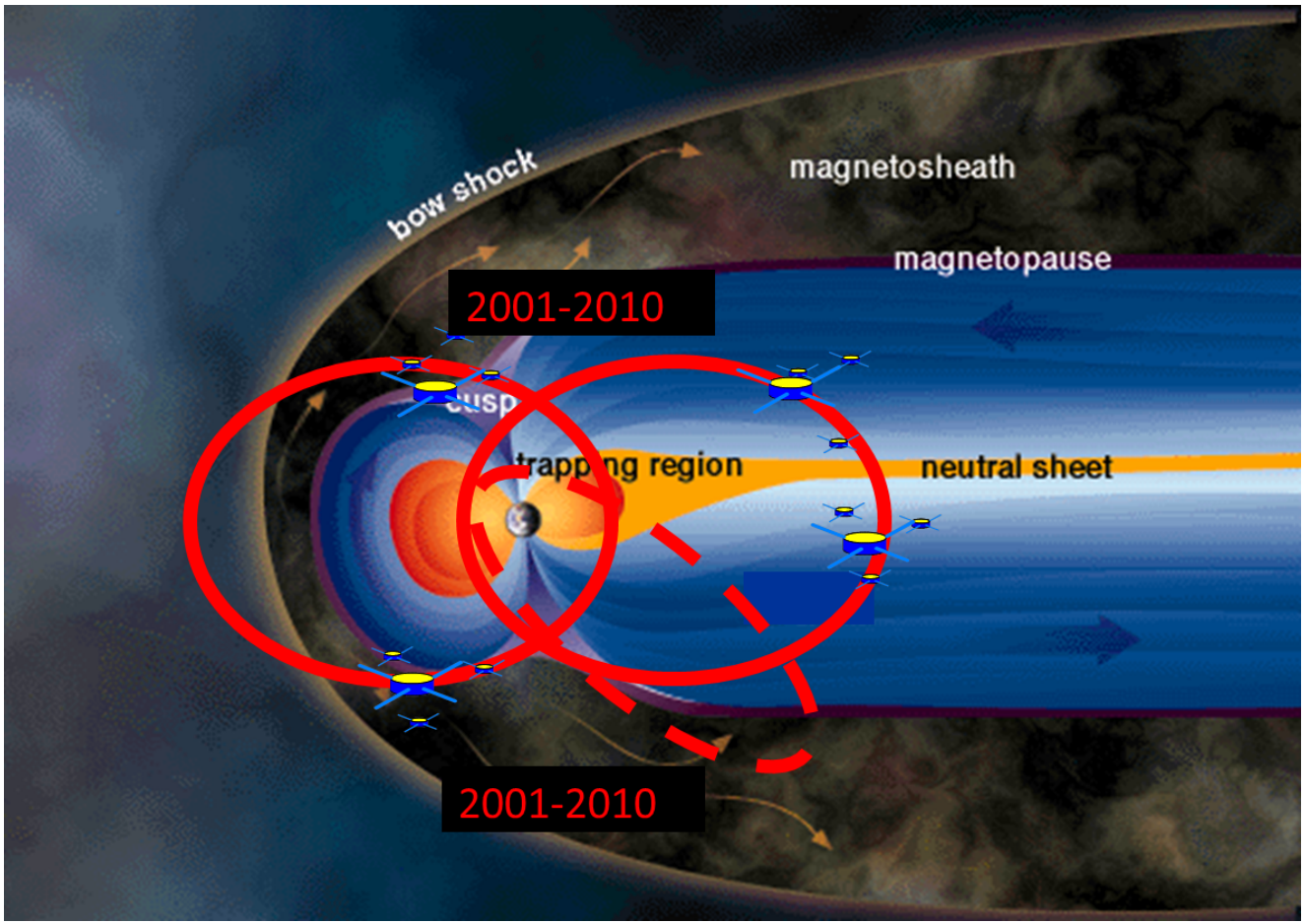

Cluster separation

"The strategy governing the separation between four spacecraft of the cluster which is varied according to the most important scale sizes of the phenomena to be studied."

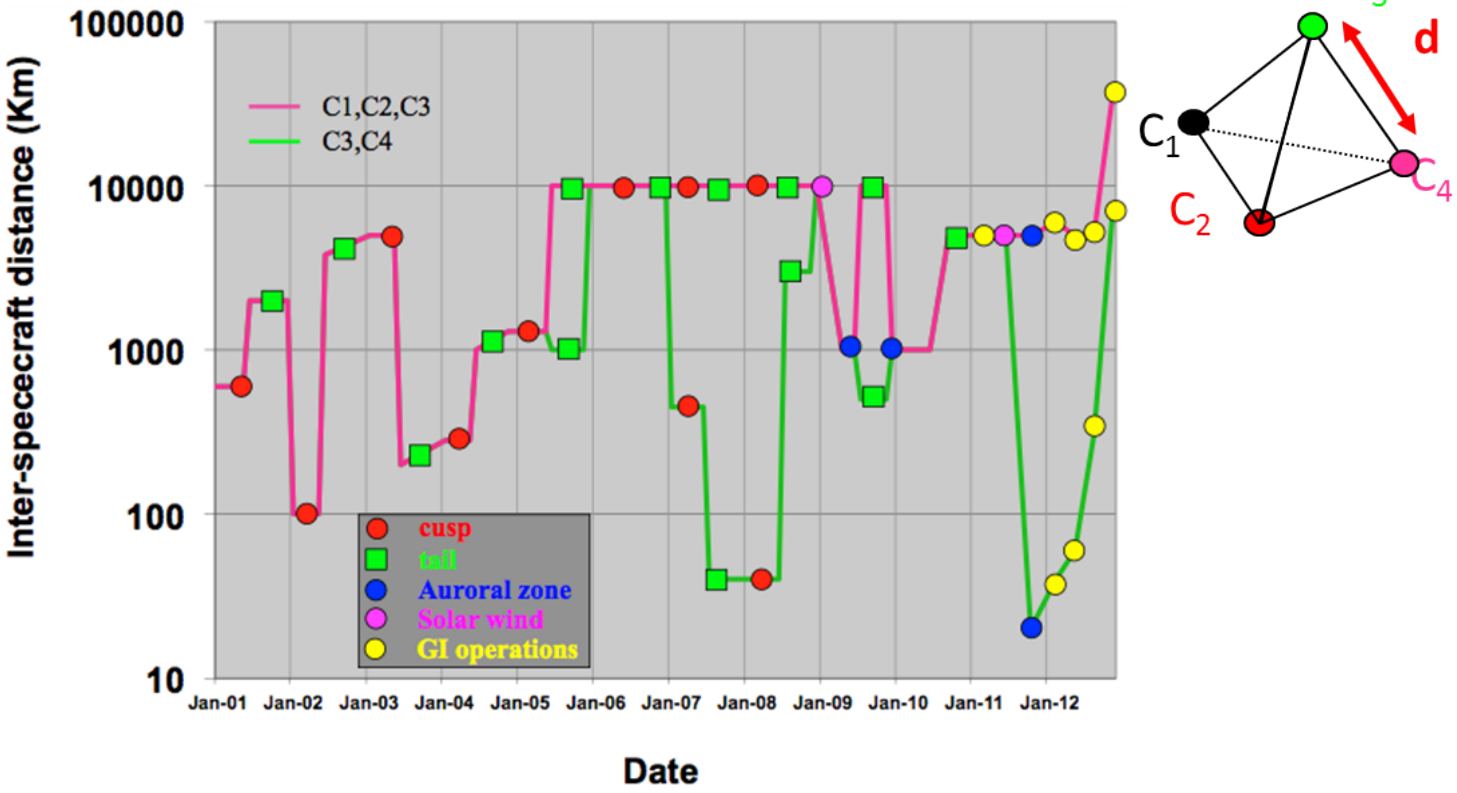

Cluster Instruments

Each of the four spacecraft are equipped with a full complement of particle and field instruments.

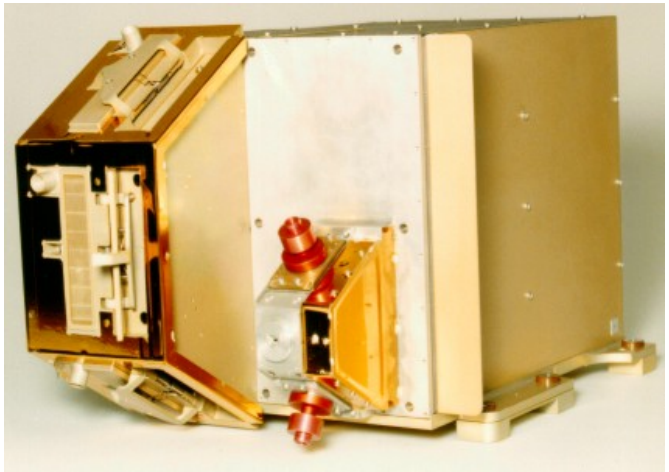

RAPID: ~30 keV – 1 MeV

CIS: ~0.01 keV – 35 keV

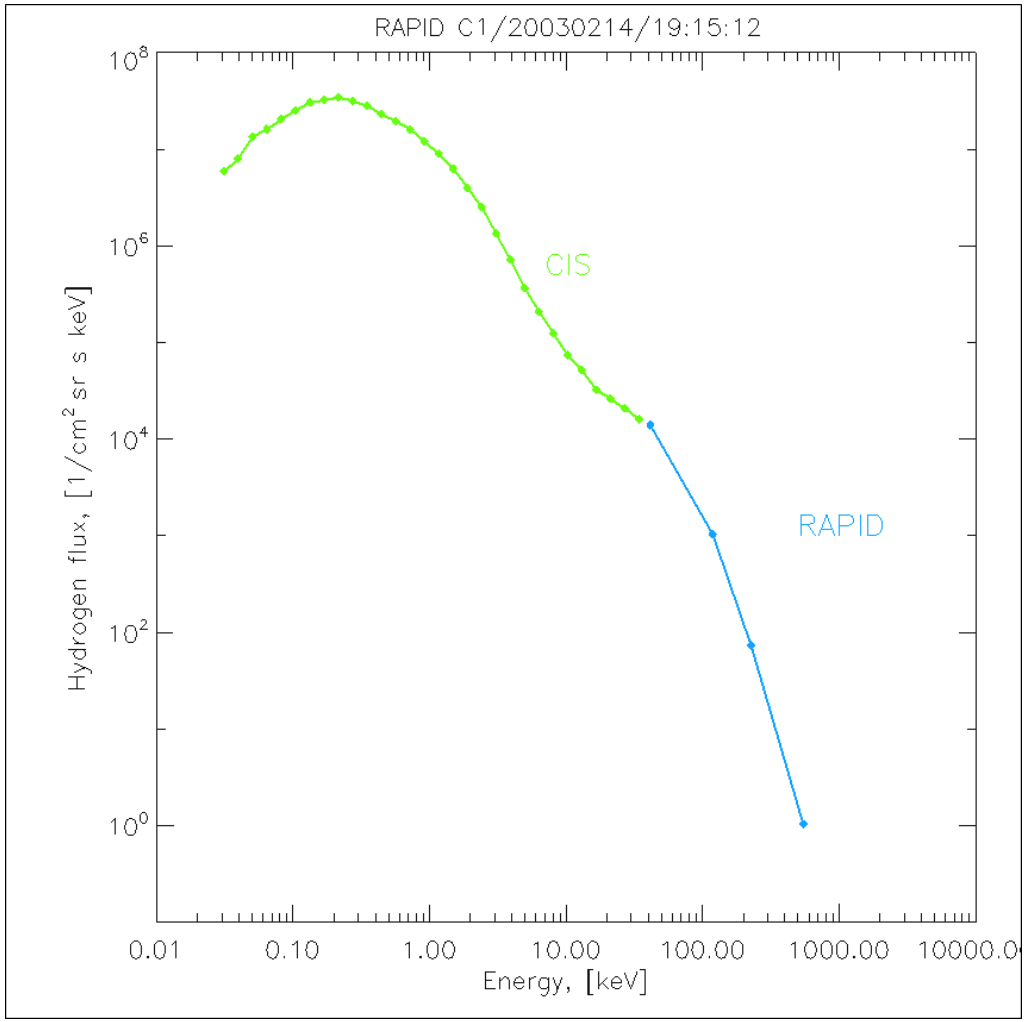

Fluxgate Magnetometer (FGM)

- Each instrument consists of two triaxial fluxgate magnetometers and onboard Data-Processing Unit (DPU)
- The mass of each sensor is 290 g + 48 g for the thermal cover.
- The mass of the electronics box is 2060 g.
- The instrument power consumption in normal operations is 2460 mW.
- In order to minimise the magnetic background of the spacecraft, one of the magnetometer sensors is located at the end of 5.2 m radial boom, the other at 1.5 m inboard from the end of the boom.
- Different ranges from -64 to +64 nT with resolution of 7.8 10^{-3} nT and from -65536 to +65528 nT with resolution of 8 nT
- Telemetry: 15.5 vector/second (Nominal mode) to 67.2 vector/second (Burst mode)

Upstream region, parallel bow shock: example CME passage, solar maximum

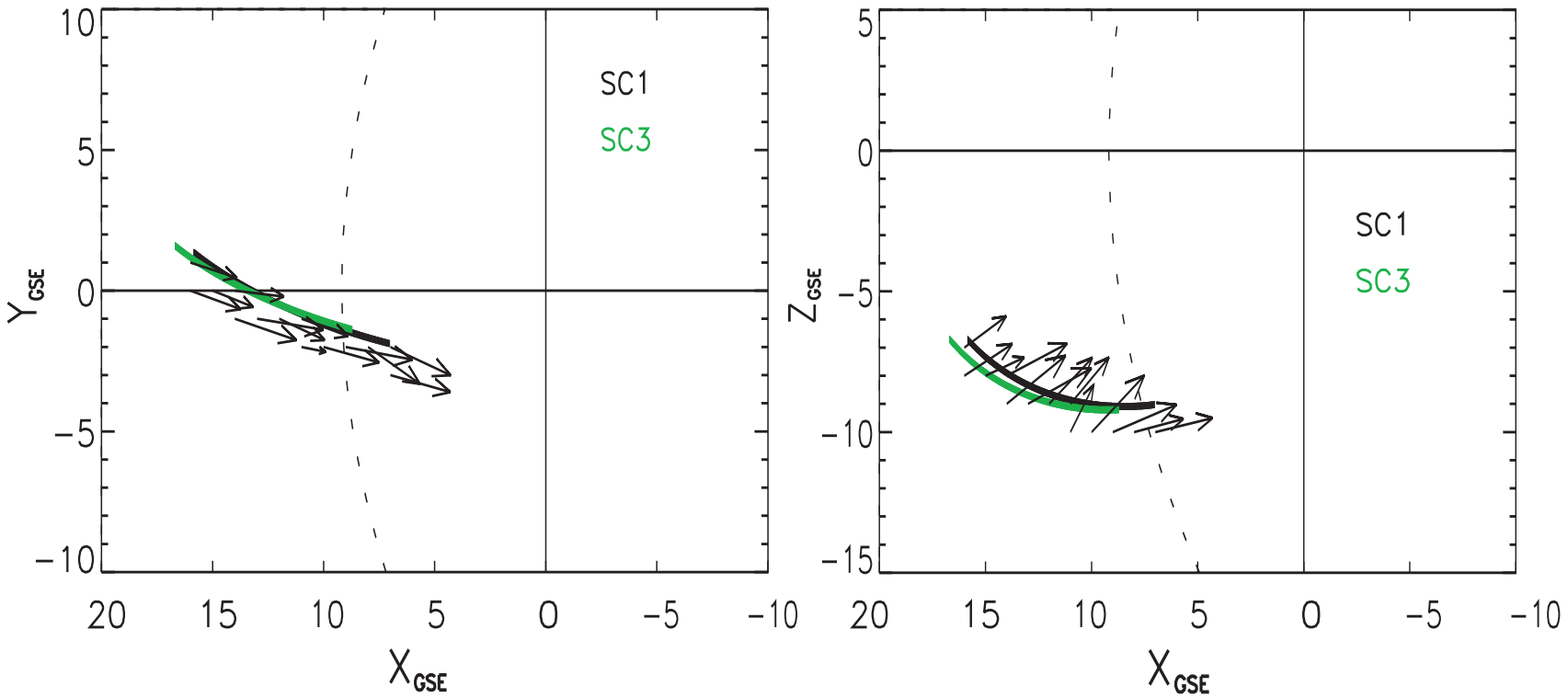

Kronberg et al., 2009

Upstream region, parallel bow shock: example

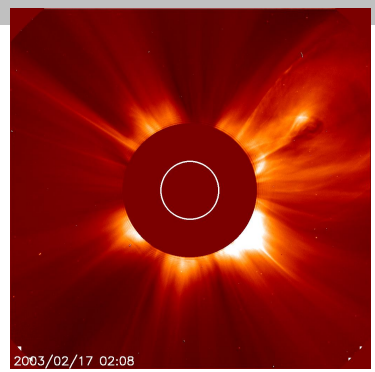

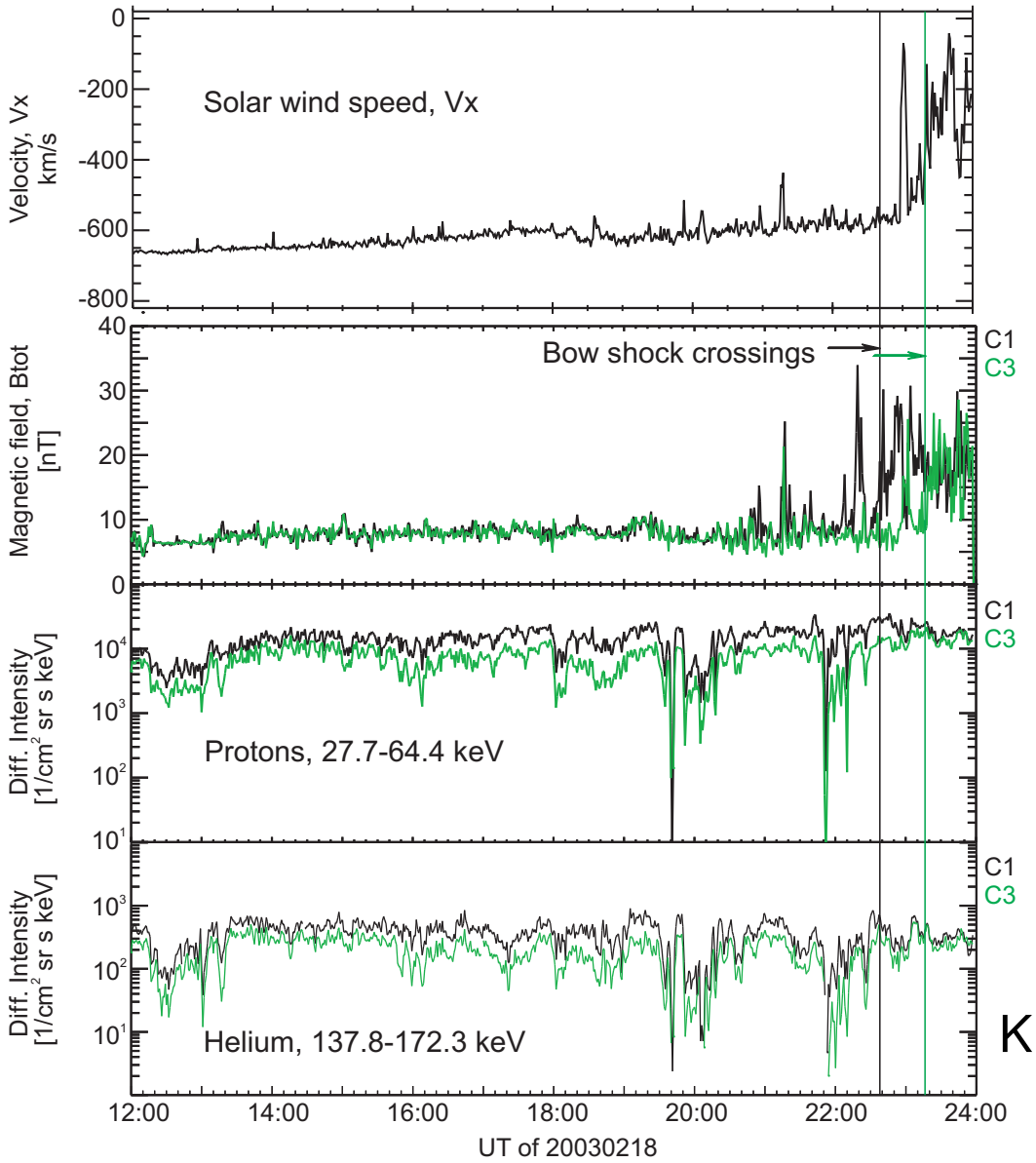

Kronberg et al., 2009

Diffusive or first order Fermi acceleration

Credit: Treumann&Jaroschek

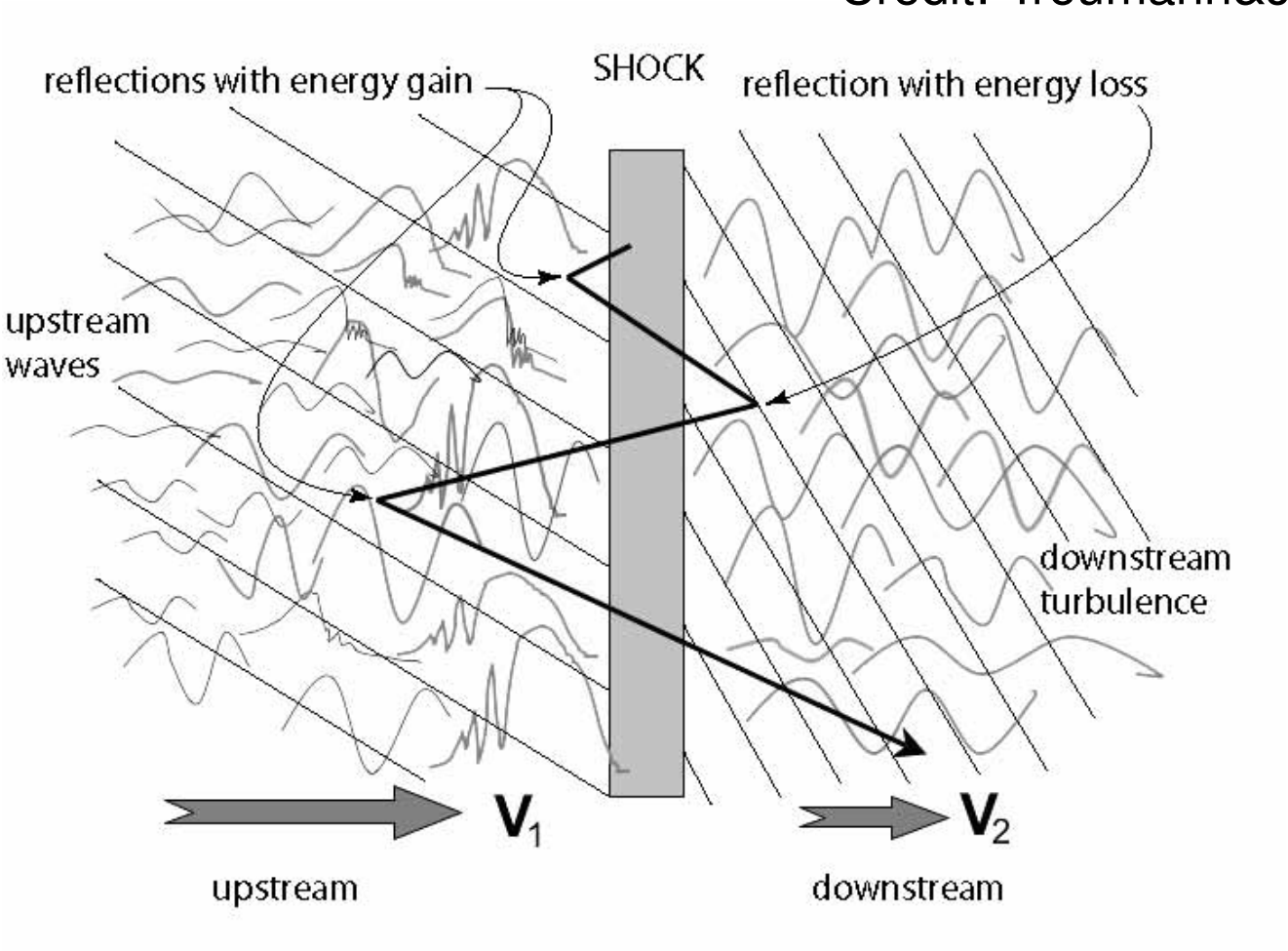

- Spatial gradient of density of upstream ions is expected to decrease exponentially with distance from the bow shock [e.g. Terasawa+81].

Upstream region: acceleration at the bow shock
CME passage, solar cycle maximum

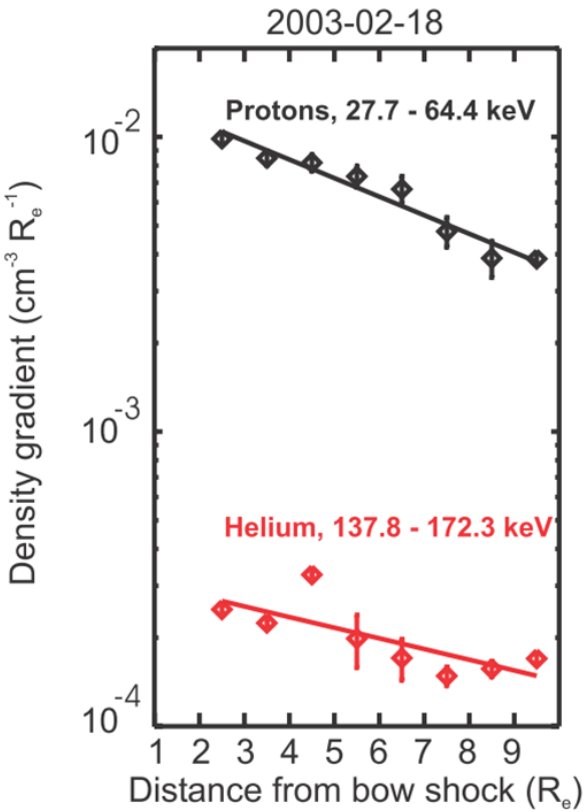

Kronberg+09

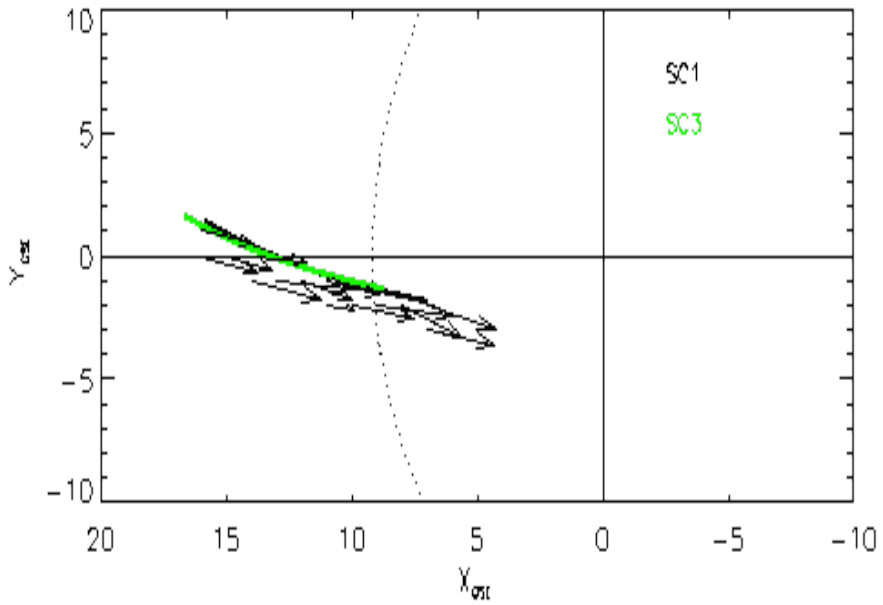

- Spatial gradient of the partial density of upstream ions is calculated.

Upstream region: acceleration at the bow shock
CME passage, solar cycle maximum

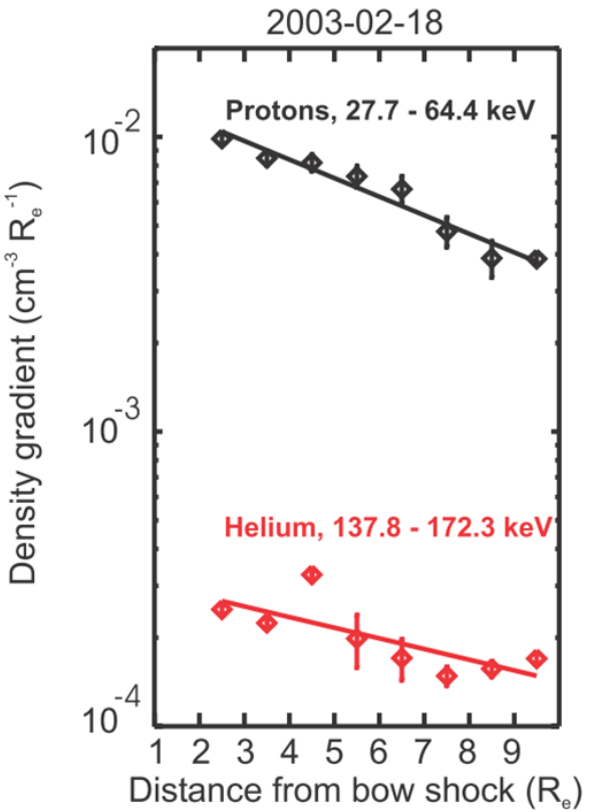

Kronberg+09

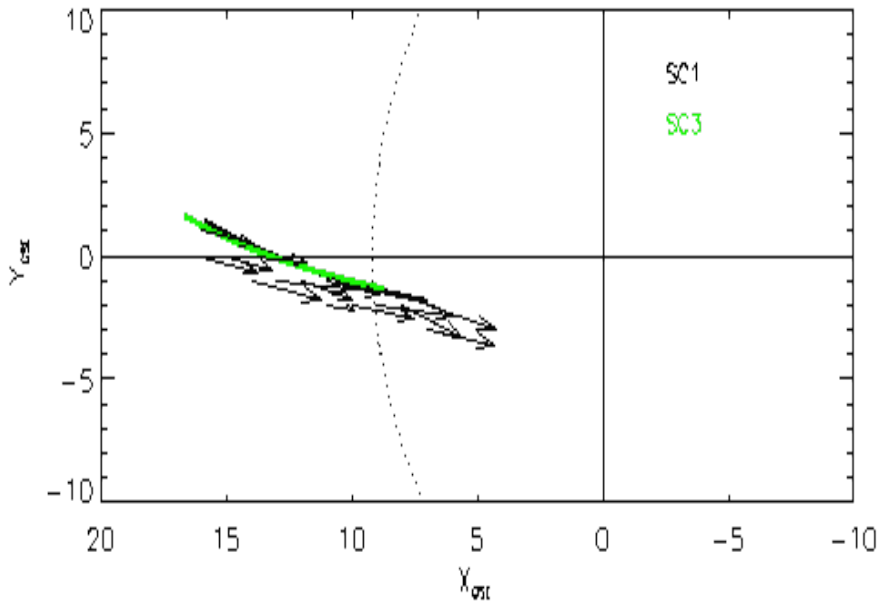

- Spatial gradient of the partial density of upstream ions is calculated.
- Scattering with waves and diffusive transport ⇒ gradients decrease exponentially with distance.

Formation of shock between solar wind streams

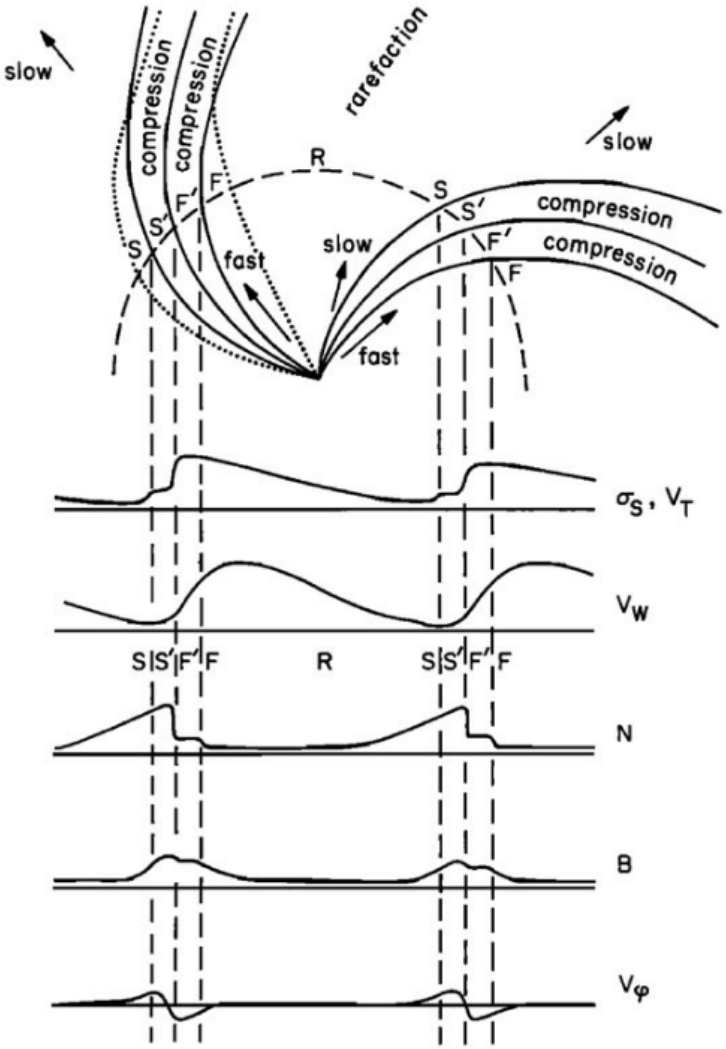

Richardson+18

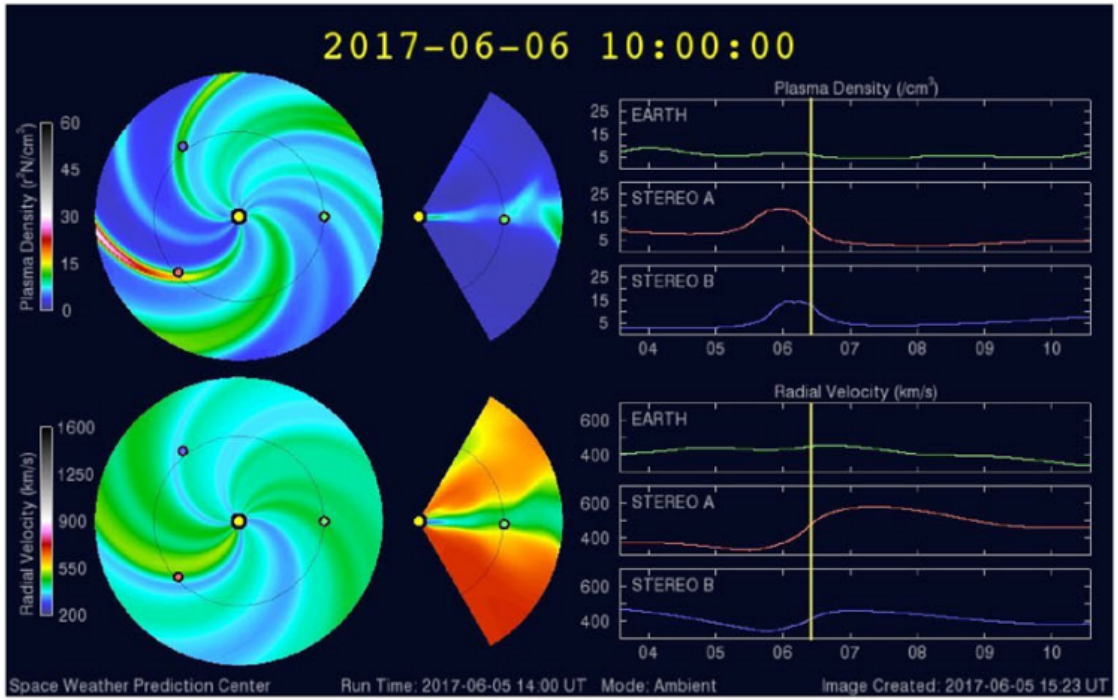

Upstream region: CIR passage, solar cycle minimum

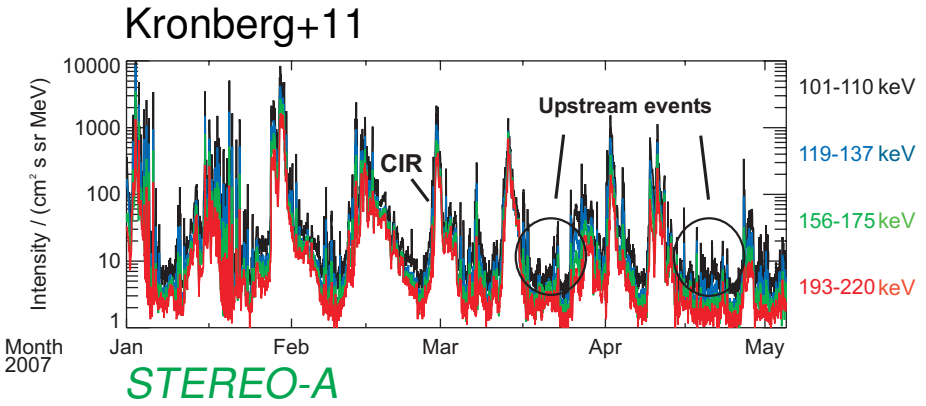

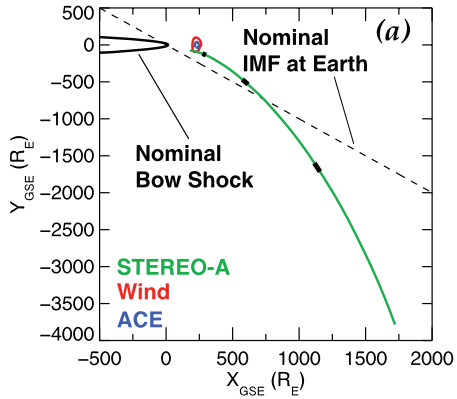

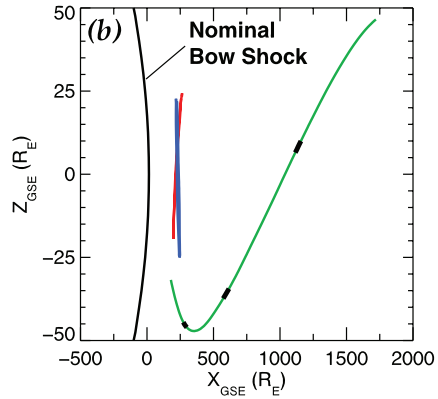

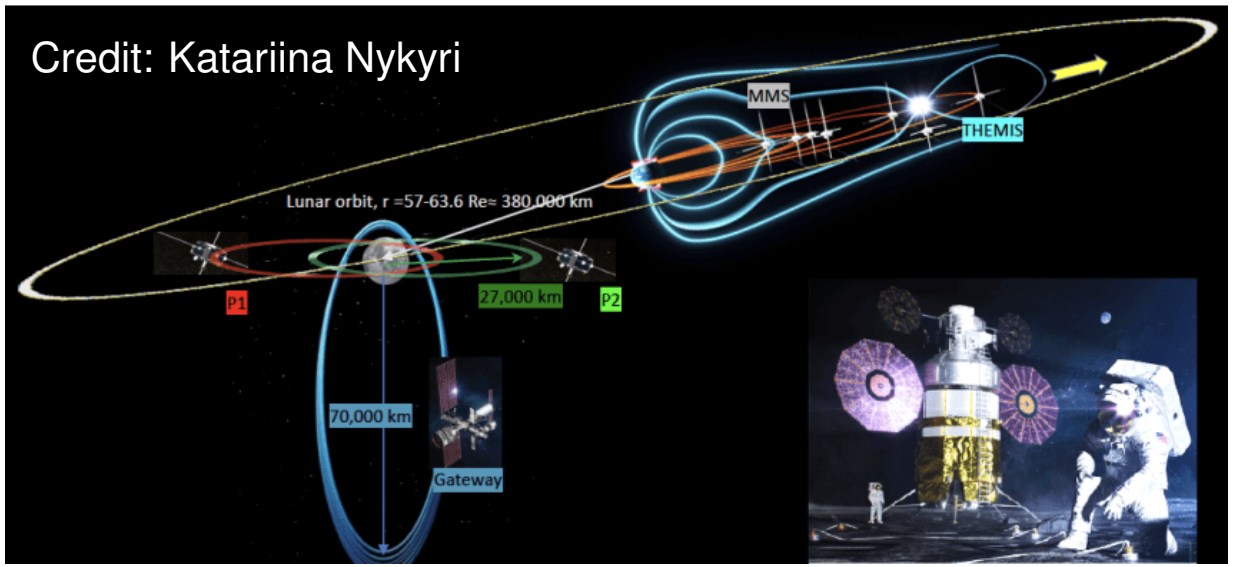

- Moon-exploration team will be affected by energetic particles in upstream region

Future applications?

Summary

- Planetary shocks are complicated structures
- They lead to strong energization of plasma which can affect the satellites.
- Energetic particles can enter into the deepest lunar wake and raise the electric potential of the lunar surface (Nishino+17). This can affect the distribution of the dust on the lunar surface and, therefore, manned activities.

Literature

- W. Baumjohann and R. Treumann, Basic Space Plasma Physics, 1996
- A. Brekke, Physics of the Upper Polar Atmosphere, 2013
- I. H. Cairns & J. G. Lyon, Magnetic field orientation effects on the standoff distance of Earth's bow shock, GRL, 23, 1996
- M. I. Desai et al., The spatial distribution of upstream ion events from the Earth's bow shock measured by ACE, Wind, and STEREO, JGR, V. 113, A08103, 2008
- H. Karimabadi, et al., The link between shocks, turbulence, and magnetic reconnection in collisionless plasmas, Physics of Plasmas, 21, 2014
- M. Kivelson and C. Russell, Introduction to Space Physics, 1995
- E. A. Kronberg, et al., Multipoint observations of ions in the 30-160 keV energy range upstream of the Earth's bow shock, JGR, 10.1029/2008JA013754, 2009
- E. A. Kronberg et al., On the origin of the energetic ion events measured upstream of the Earth's bow shock by STEREO, Cluster, and Geotail, JGR, 10.1029/2010JA015561, 2011
- M. N. Nishino et al., Kaguya observations of the lunar wake in the terrestrial foreshock: Surface potential change by bow-shock reflected ions, Icarus, doi: 10.1016/j.icarus.2017.04.005, 2017

Literature

- F. Menk and C. Waters, Magnetoseismology: Ground-based remote sensing of Earth's magnetosphere, 2013
- M. Peredo et al., Three-dimensional position and shape of the bow shock and their variation with Alfvenic, sonic and magnetosonic Mach numbers and interplanetary magnetic field orientation, JGR, 100, 1995
- T. Terasawa, Energy spectrum of ions accelerated through Fermi process at the terrestrial bow shock, JGR, vol. 86, 1981
- R. A. Treumann & C. H. Jaroschek, Fundamentals of Non-relativistic Collisionless Shock Physics: V. Acceleration of Charged Particles, ARXIV [astro-ph], 2008